

# Detection of Biological Analytes at Physiological Conditions using Localized Surface Plasmon Resonance Spectroscopy

*Undergraduate Researcher*  
Jessica A. Huber, St. Louis University

*Faculty Mentor*  
Richard P. Van Duyne  
Department of Chemistry, Northwestern University

*Graduate Student Mentors*  
Erin McLellan Hicks and Chanda Ranjit Yonzon  
Department of Chemistry,  
Northwestern University

## Abstract

This work exploits the use of noble metal nanoparticles to achieve sensitive and selective detection of chemical and biological analytes. The localized surface plasmon resonance (LSPR) of these metal nanoparticles is known to be sensitive to shape, size, and the local environment. Ag nanoparticles fabricated using the nanosphere lithography (NSL) technique exploit this LSPR sensitivity as a signal transduction method in biosensing applications. Current work strives to investigate the impact of changing the nanoparticle aspect ratio on the solvent sensitivity of the assay and to implement LSPR biosensing in a dinitrophenyl (DNP) derivative immunoassay system. Antidinitrophenyl (antiDNP) is an analog of trinitrotoluene (TNT). Thus, the antiDNP binding study will provide enormous insight into the detection of chemical warfare reagents. In studying the impact of particle aspect ratio on sensitivity, it was found that for a 390 nm diameter nanosphere mask, the particles with the shortest height, 15 nm, demonstrated the highest sensitivity, 265.44 nm RIU<sup>-1</sup> [(refractive index unit)<sup>-1</sup>]. Upon formation of the DNP/antiDNP complex in phosphate buffered water, the system showed an average LSPR shift of 15 nm for a particle height of 25 nm. Further nonspecific binding studies showed high analyte specificity in three separate cases: when the DNP

derivative was not attached, when bovine serum albumin (BSA) was introduced, and in a mixture of BSA and the DNP derivative.

## Introduction

A means for detecting molecules quickly, accurately, and at low concentrations is in high demand. The employment of triangular silver nanoparticles as sensing platforms proves to be highly selective at naturally occurring concentrations.<sup>1-4</sup> Using LSPR, silver nanosensors are able to perform parallel screening of multiple interactions and exhibit efficient results.<sup>4</sup>

Noble metal nanoparticles such as gold and silver are unique in that upon excitation, they exhibit collective oscillations of the surface electrons, which is called

the localized surface plasmon resonance (LSPR). LSPR is the extinction (absorbance and Rayleigh scattering) band that results when the collective oscillation of surface electrons are resonant with the incident photon frequency. The peak extinction wavelength of the band,  $\lambda_{\text{max}}$ , can be measured through a variety of techniques. The most common technique for silver nanoparticles is UV (vis) spectroscopy.<sup>1,5-10</sup>

As previously mentioned, at the LSPR, metal nanoparticles strongly absorb and scatter light. The observed color of the metal particles is a direct result of the ratio of scattering to absorption. Smaller particles tend to absorb light more intensely, whereas the color of larger particles is due primarily to scattering.

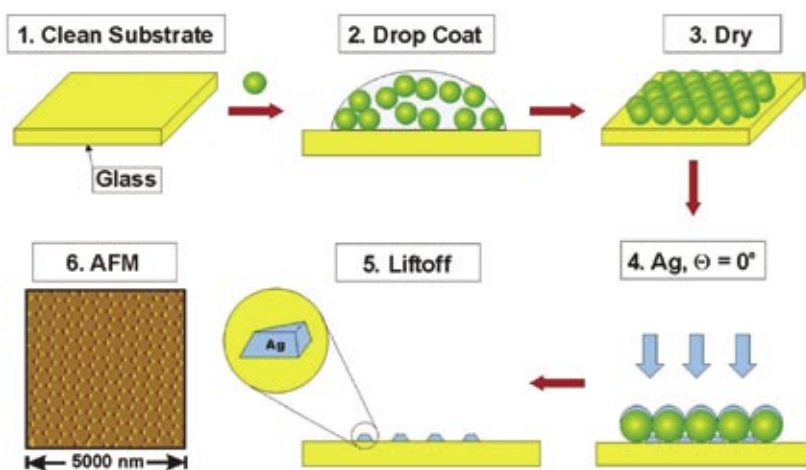


**Figure 1:** Fabrication of triangular Ag nanoparticles through nanosphere lithography (NSL). (1) Glass substrates are cleaned with piranha etch and rendered hydrophilic with a base treatment. (2) A polystyrene nanosphere solution is drop coated onto the substrate. (3) The nanosphere solution forms hexagonally packed array. (4) Deposition of Ag onto the nanosphere mask. (5) Removal of sphere through sonication, leaving an array of triangular Ag nanoparticles. (6) ARM image taken of Ag nanoparticles.

## Detection of Biological Analytes at Physiological Conditions Using Localized Surface Plasmon Resonance Spectroscopy (continued)

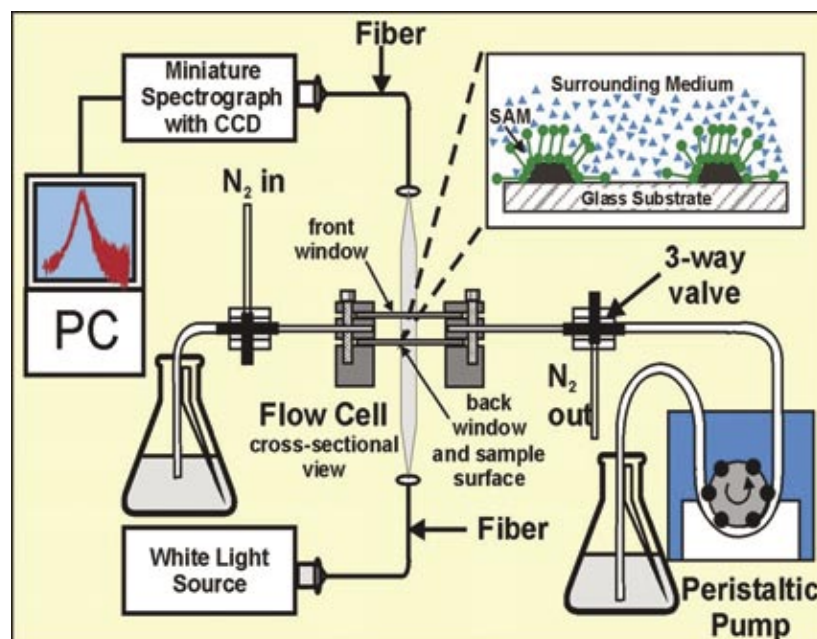


**Figure 2:** Instrumental diagram of LSPR sensor experiment. The substrate-bound nanoparticles sandwiched within the flow cell emit an extinction wavelength when excited by the white light source. The wavelength is then measured by a spectrograph with CCD. The inset shows a schematic diagram of the SAM-modified nanoparticles in a surrounding medium — either solvent, buffer, or gas.

The optical properties of noble metal particles have been exploited for several centuries. Uses include the staining of glass windows and the creation of metal chalices.<sup>5</sup> Recently, noble metal nanoparticles have found many more uses in the area of biological sciences, such as biosensor devices.

Mie theory is the simplest theoretical model that rationalizes the optical properties of metal nanoparticles and is described by Equation 1,

$$E(\lambda) = \frac{24\pi N_A a^3 \epsilon_m^{3/2}}{\lambda \cdot \ln(10)} \left[ \frac{\epsilon_i}{(\epsilon_r + \chi \epsilon_m)^2 + \epsilon_i^2} \right]$$

- $E(\lambda)$  = extinction
- $N_A$  = areal density of nanoparticles
- $A$  = radius of metallic nanosphere
- $\epsilon_m$  = dielectric constant of the surrounding medium
- $\lambda$  = wavelength of absorbing radiation
- $\epsilon_i$  = imaginary portion of the metallic nanoparticle's dielectric constant
- $\epsilon_r$  = real portion of the metallic nanoparticle's dielectric constant
- $\chi$  = shape factor term that describes the nanoparticle's aspect ratio (2 for a sphere)

The theory predicts that the size, shape, material, and dielectric environment of the nanoparticles determine the LSPR  $\lambda_{max}$ . By the theory, this means that changes in the local dielectric environment caused by binding events cause a shift in the peak extinction wavelength,  $\lambda_{max}$ . Henceforth, any binding events will also inevitably shift the LSPR  $\lambda_{max}$ , providing a great tool as a chemo- or biosensor.<sup>1,8,11-13</sup>

In order to develop such applications, it is necessary to find a method to produce large quantities of robust nanoparticle platforms that can be used in various biological studies. NSL is a low-cost, parallel, surface-independent technique used for producing well-ordered array structures with nanometer precision. NSL is based on the self-assembly of polystyrene or silica nanospheres into hexagonally close-packed monolayer and multilayer structures. These structures are then used as lithographic masks for etching or deposition, creating an array of truncated tetrahedral nanoparticles.<sup>14</sup> The size and interhole spacing of nanoparticles can be tuned by using different sphere sizes, metal thicknesses, and etch times.<sup>6,13</sup>

Here, we describe a series of three studies: (1) A solvent study was performed to emphasize the effect the surrounding medium has on the extinction spectrum of the nanoparticles. (2) A binding study of antiDNP was performed at physiological conditions to demonstrate nanoparticles' ability to detect biomolecules. (3) Finally, a nonspecific binding study was conducted to show that the nanoparticle array exhibited few nonspecific interactions.

## Background

Previously, SPR-based sensors were the prevalent technique used to detect biological analytes on functionalized surfaces.<sup>6,15,16</sup> SPR occurs when a light beam hits a half-circular prism coated with a thin film of noble metal. The angle of resonance is dependent on the refractive index of the adsorbate and is measured with a CCD-chip. The Van Duyne group at Northwestern University has recently developed LSPR sensors that resolve the challenges presented by SPR sensors while maintaining comparable sensitivity.<sup>2-4,17</sup> They have a small pixel size due to the single nanoparticle platform, demand simple construction, require small sample volumes, and exhibit short-range distance dependence. In addition, LSPR systems cost less than \$5,000, compared with the commercialized SPR instruments, which range from \$150,000 to \$300,000.<sup>1,4,8,10</sup>

With this new sensor, it is necessary to identify model systems to use as a basis to analyze the potential of new sensors and compare them with sensors that are already out there. The three ligand/receptor systems that have been studied to demonstrate the potential of LSPR sensors are biotin/streptavidin, biotin/antibiotin, and Concanavalin A/mannose. The biotin/streptavidin system, with its extremely high binding affinity ( $K_a \sim 10^{13}$  1/M), illustrates the ultrasensitive attributes of LSPR-based nanoscale affinity biosensors. The schematic involved the formation of a self-assembled monolayer, SAM, on the Ag nanoparticles, followed by the covalent attachment of biotin. The LSPR  $\lambda_{\text{max}}$  was measured after each step: bare Ag nanoparticles, 561.4 nm; SAM, 598.6 nm, a 38 nm red shift; and biotin, 609.6 nm, a 11 nm red shift.

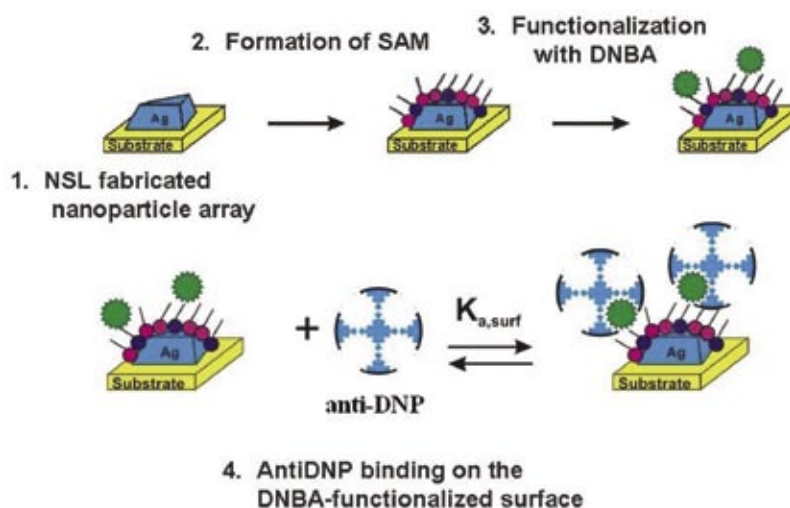


**Figure 3: Schematic representation of antiDNP binding to a DNBA-functionalized Ag nanosensor fabricated by NSL.**

Finally, after exposure to 100 nM of the streptavidin protein, the LSPR  $\lambda_{\text{max}}$  experienced an additional 27 nm shift to 636.6 nm.<sup>1,8</sup>

The biotin/antibiotin immunoassay demonstrated the LSPR biosensing capabilities with biological couples whose binding affinity is significantly lower ( $1.9 \times 10^6 - 4.98 \times 10^8$  1/M) than the biotin/streptavidin system's. The formation of the SAM resulted in a LSPR  $\lambda_{\text{max}}$  of 670.3 nm. After biotin binding, the LSPR extinction wavelength of the Ag nanoparticles was measured at 683.0 nm, a red shift of 12.7 nm. Following incubation in 700 nM antibiotin, the Ag nanoparticles displayed a LSPR  $\lambda_{\text{max}}$  of 725.6 nm, a 42.6 nm red shift.<sup>1,8</sup>

The Concanavalin A (Con A)/mannose system was used for the comparative analysis of a NSL-fabricated Ag nanoparticle LSPR sensor and a planar thin film

Au SPR sensor. The study was accomplished by comparing the SPR response ( $\Delta\theta$ ) and the LSPR response ( $\Delta\lambda$ ) with the binding of Con A to the SAM. The SPR angle shifts and LSPR wavelength shifts experienced comparable magnitude saturation coverage responses during the association phase when Con A specifically bound to the mannose-functionalized surface. However, during the removal of weakly bound Con A during the dissociation phase, the SPR sensor showed approximately five times' greater response than the LSPR sensor. This is due to the fact that the sensing distance of the LSPR sensor is shorter than that of the SPR sensor, resulting in a smaller shift. In summary, this study shows that LSPR-based biosensors are comparable to those currently on the market.<sup>4,8</sup>

Detection of Biological Analytes at Physiological Conditions  
Using Localized Surface Plasmon Resonance Spectroscopy (*continued*)

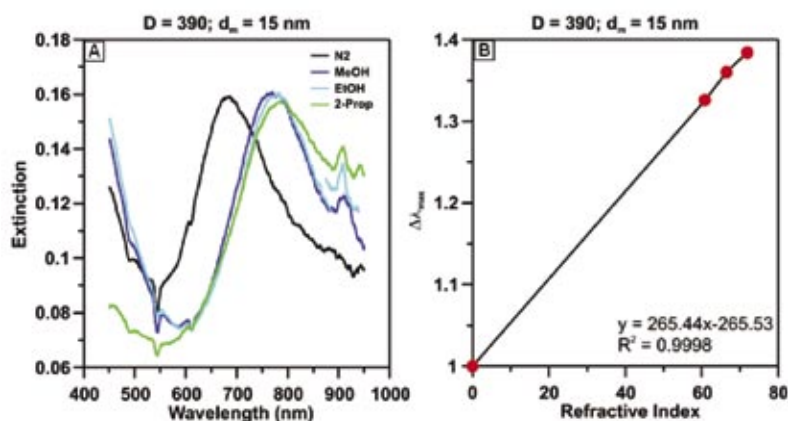


Figure 4: Binding study with 15 nm height Ag particles. (a) LSPR shifts when methanol, ethanol, and 2-propanol were exposed to the nanoparticle array. (b) LSPR  $\lambda_{max}(\text{solvent}) - \lambda_{max}(\text{dry N}_2)$  versus the refractive index of the solvent. There is a linear relationship between the solvent refractive index and the nanoparticle's  $\lambda_{max}$ .

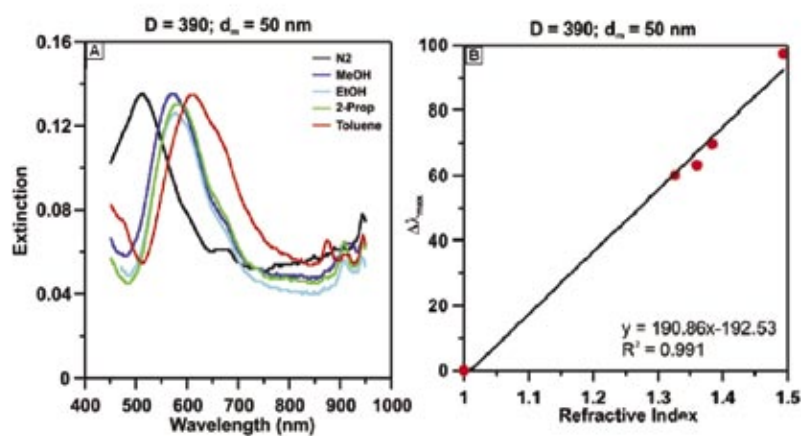


Figure 5: Binding study with 50 nm height Ag particles. (a) LSPR shifts when methanol, ethanol, 2-propanol, and toluene are exposed to the nanoparticle array. (b) LSPR  $\lambda_{max}(\text{solvent}) - \lambda_{max}(\text{dry N}_2)$  versus the refractive index of the solvent. There is a linear relationship between the solvent refractive index and the nanoparticle's  $\lambda_{max}$ .

### Approach

#### Fabrication of Ag Nanoparticles: NSL

The fabrication of the triangular Ag nanoparticles was achieved through NSL (Figure 1). The technique begins with the pretreatment of glass substrates in two steps: (1) piranha etch, 1:3 30% H<sub>2</sub>O<sub>2</sub>:H<sub>2</sub>SO<sub>4</sub>, for .5 hr to clean the substrate, and (2) base treatment, 5:1:1 H<sub>2</sub>O:NH<sub>4</sub>OH:30% H<sub>2</sub>O<sub>2</sub> with sonication, for 1 hr to render the surface hydrophobic. Approximately 2  $\mu$ l of a carboxyl-substituted polystyrene latex nanosphere solution, containing 390 nm spheres, was drop-coated onto the glass substrate. The nanosphere solution was allowed to dry at ambient conditions to form a hexagonally packed array. A desired height of Ag was then deposited onto the nanosphere mask. The polystyrene nanospheres were removed by sonication in absolute ethanol for about 3 min, leaving an array of triangular Ag nanoparticles.

#### Solvent Study: Confirmation of Ag Nanoparticle Sensitivity

Nanoparticle are extremely sensitive to the refractive index of the surrounding medium. To study this effect, a solvent study was performed. Two out-of-plane Ag heights were used for the samples: 15 and 50 nm. The substrate-bound Ag nanoparticles were sandwiched inside a custom-built flow cell shown in Figure 2. To stabilize the nanoparticles, methanol followed by dry N<sub>2</sub> gas was cycled through the flow cell until the UV-vis spectrum repeatedly returned to the same spectral location in N<sub>2</sub>. The relationship between the LSPR  $\lambda_{max}$  and the external dielectric constant was examined by immersing the nanoparticle samples in a variety of solvents. These solvents represent a progression of refractive indices: nitrogen (RI=1.0), methanol

(1.326), ethanol (1.36), 2-propanol (1.384), and toluene (1.494). Each sample was equilibrated in a  $N_2$  environment between solvent treatments.

*AntiDNP Binding Study: Ability of Ag Nanoparticles to Detect Biomolecules*

Figure 3 shows the schematic used to functionalize the antiDNP system. Three out-of-plane Ag heights were used for the nanotriangles: 15, 25, and 50 nm. The nanotriangles were first exposed to a 1 mM 2:1 octanethiol: 11-aminoundecanethiol for 48 hr to ensure a well-ordered self-assembled monolayer (SAM). Octanethiol was used as a packing material, while 11-aminoundecanethiol was used to covalently attach 2,4-dinitrobenzoic acid (DNBA) using 1-ethyl-3-[3-dimethylamino-propyl]carbodiimide hydrochloride (EDC) as a coupling reagent. The covalent attachment of DNBA was accomplished by exposing the SAM-functionalized nanoparticles to 1mM DNBA and 1mM EDC for 3 hr to form an amide bond. The immunoassay was performed by incubating the DNBA-modified sample in a  $1.05 \times 10^{-7}$  M and  $4.912 \times 10^{-6}$  M antiDNP solution for 30 min.

*Nonspecific Binding Study: Confirmation of Ag Nanoparticle Selectivity*

It is important for a nanosensor to have very few nonspecific interactions. To verify the selectivity of the nanoparticle array, three different cases of a nonspecific binding study were performed, using nanoparticles with an out-of-plane height of 15 nm.

*(1) AntiDNP Activity with the SAM Only: No Functionalized-DNBA Surface.*

The Ag nanoparticles were incubated in the SAM as before. However, the nanoparticles were not exposed to the

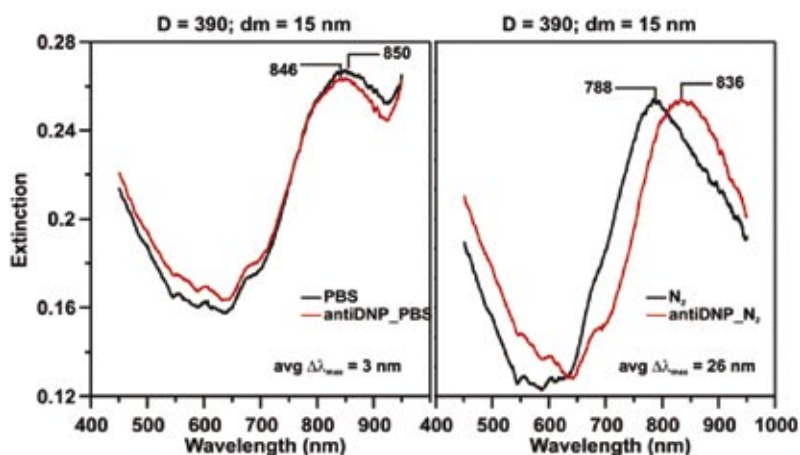


Figure 6: LSPR response to  $1.05 \times 10^{-7}$  M antiDNP binding to the DNBA-functionalized Ag nanoparticles with out-of-plane height of 15 nm. (a) LSPR measurements taken in PBS before and after incubation in antiDNP. (b) LSPR measurements taken in dry  $N_2$  before and after incubation in antiDNP.

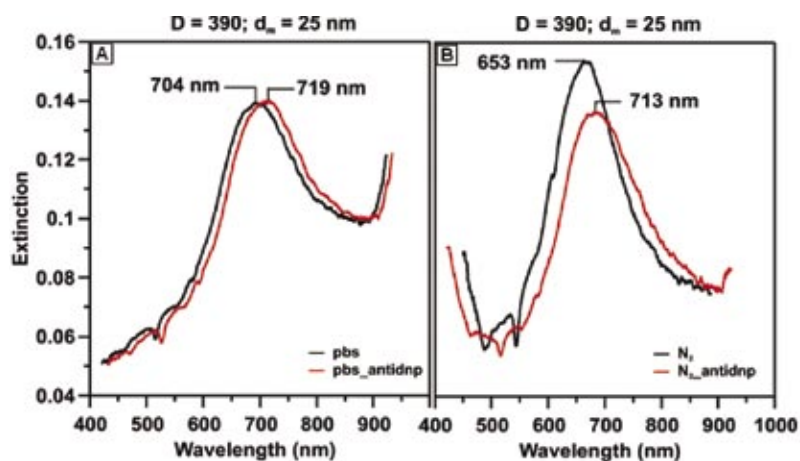


Figure 7: LSPR response to  $4.912 \times 10^{-6}$  M antiDNP binding to the DNBA-functionalized Ag nanoparticles with out-of-plane height of 25 nm. (a) LSPR measurements taken in PBS before and after incubation in antiDNP. (b) LSPR measurements taken in dry  $N_2$  before and after incubation in antiDNP.

Detection of Biological Analytes at Physiological Conditions  
Using Localized Surface Plasmon Resonance Spectroscopy (*continued*)

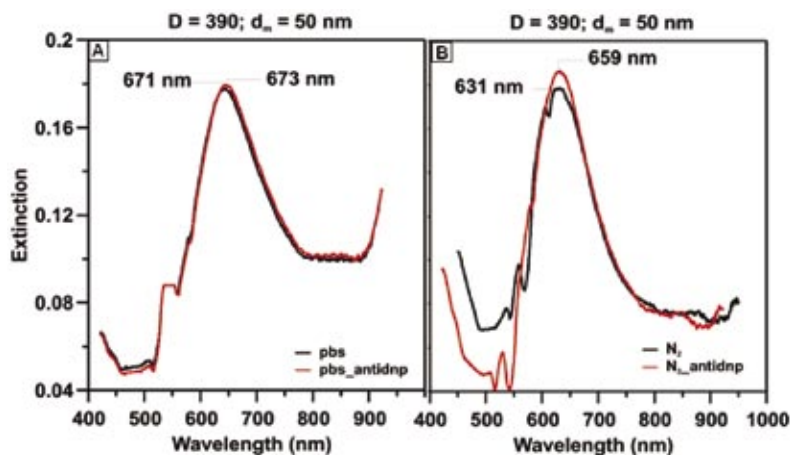


Figure 8: LSPR response to  $4.912 \times 10^{-6}$  M antiDNP binding to the DNBA-functionalized Ag nanoparticles with out-of-plane height of 50 nm. (a) LSPR measurements taken in PBS before and after incubation in antiDNP. (b) LSPR measurements taken in dry N<sub>2</sub> before and after incubation in antiDNP.

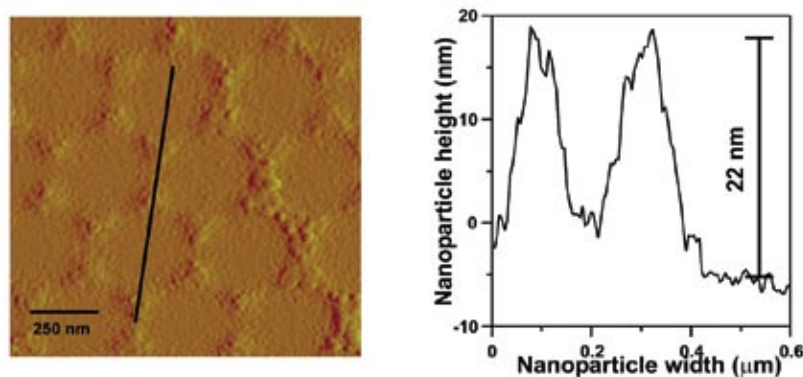


Figure 9: AFM tapping mode image and line scans of Ag nanosensors used to study the height increment after functionalizing with SAM (height = 7 nm). The Ag nanosensors were fabricated from hexagonal arrays of 390 nm diameter polystyrene spheres and 15 nm Ag deposition.

DNBA/EDC solution prior to incubation in antiDNP. This case demonstrated that Ag nanosensors require the proper biological couple for the binding event to occur.

(2) *Bovine Serum Albumin (BSA) Interaction with the DNBA-Functionalized Sensor.* The DNBA-functionalized Ag nanosensors were exposed to a 1 mg/mL solution of BSA to demonstrate that the nanoparticles do not exhibit an affinity toward other molecules.

(3) *Specific Sensing in the Presence of an Interfering Molecule.* The DNBA-functionalized Ag nanoparticles were exposed to a 1:1 solution of BSA and antiDNP. It is crucial to show specific antiDNP binding in the presence of an interfering molecule.

## Results and Discussion

*Solvent Study: Ag Nanoparticle Sensitivity*  
Two different heights of nanoparticles were used to identify the relationship between nanoparticle height and refractive index sensitivity.

First, the LSPR spectrum of the 15 nm height Ag nanosensor in N<sub>2</sub> had a  $\lambda_{\max}$  of 683.22 nm. Injection of MeOH, EtOH, and 2-propanol resulted in a  $\lambda_{\max}$  of 769.23 nm, 778.37 nm, and 785.75 nm respectively and is shown in Figure 4A. As illustrated in Figure 4B, the LSPR  $\lambda_{\max}$  systematically shifts to longer wavelength as the solvent refractive index unit (RIU) is increased. A linear fit to the plot of  $\Delta\lambda_{\max}$  versus the refractive index of the media results in a refractive index sensitivity of 265.44 nm RIU<sup>-1</sup>.

Second, a Ag nanosensor with an out-of-plane height of 50 nm in N<sub>2</sub> had a measured  $\lambda_{\max}$  of 511.89 nm. The solvents MeOH, EtOH, 2-propanol, and

toluene were injected into the flow cell and rendered  $\lambda_{\text{max}}$  values of 572.70 nm, 578.33 nm, 583.78 nm, and 611.49 nm respectively (Figure 5A). Figure 5B shows the linear relationship between the  $\lambda_{\text{max}}$  and solvent RIU, yielding a sensitivity of 190.85 nm RIU<sup>-1</sup>.

The study shows that not only are the nanoparticles directly affected by their surroundings, but also that the shorter out-of-plane height Ag particles are more sensitive to changes in the surrounding dielectric medium. Higher refractive index sensitivities signify that particles with smaller out-of-plane heights show greater shifts when the refractive index of their surroundings are changed.

#### *AntiDNP Binding Study: Detection of Biomolecules*

To study the selectivity and sensitivity of nanobiosensors produced by NSL, three different nanoparticle heights were studied: 15, 25, and 50 nm.

The LSPR response of the 15 nm height nanosensor to a  $1.05 \times 10^{-7}$  M antiDNP solution is shown in Figure 6. The  $\lambda_{\text{max}}$  of the DNBA-functionalized nanoparticles was measured to be 788 nm in N<sub>2</sub>. After the sample was exposed to PBS, the measured LSPR  $\lambda_{\text{max}}$  was 846 nm. The sample was then incubated in antiDNP for 30 min. When the sample was again exposed to PBS, the  $\lambda_{\text{max}}$  shifted to 850 nm. The nanoparticle array was rinsed with pH adjusted (~7) water before drying in N<sub>2</sub>. The final extinction measurement was then measured to be 836 nm. The shifts caused by the binding event were 4 nm in PBS (Figure 6A) and 48 nm in N<sub>2</sub> (Figure 6B).

The 25 nm height samples exhibited  $\lambda_{\text{max}}$  values of 653 nm in N<sub>2</sub> and 704 nm in PBS prior to exposure to  $4.912 \times 10^{-6}$  M

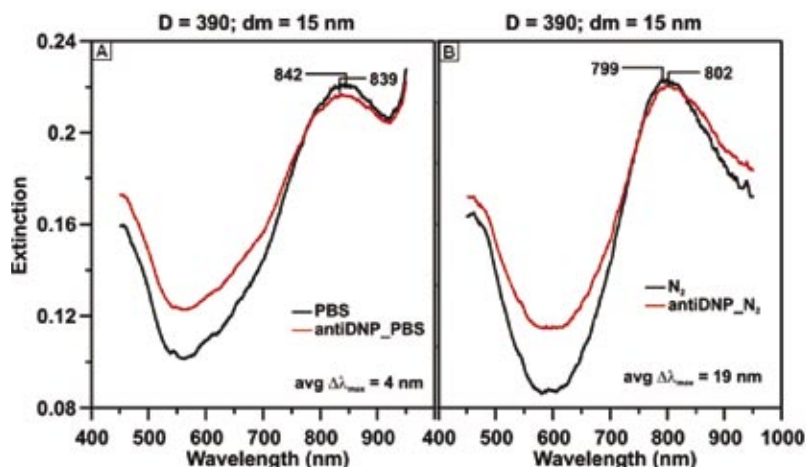


**Figure 10:** Nonspecific binding study on SAM-functionalized Ag nanosensor. (a) LSPR measurements taken in PBS before and after incubation in  $1.05 \times 10^{-7}$  M antiDNP. (b) LSPR measurements taken in dry N<sub>2</sub> before and after incubation in antiDNP.

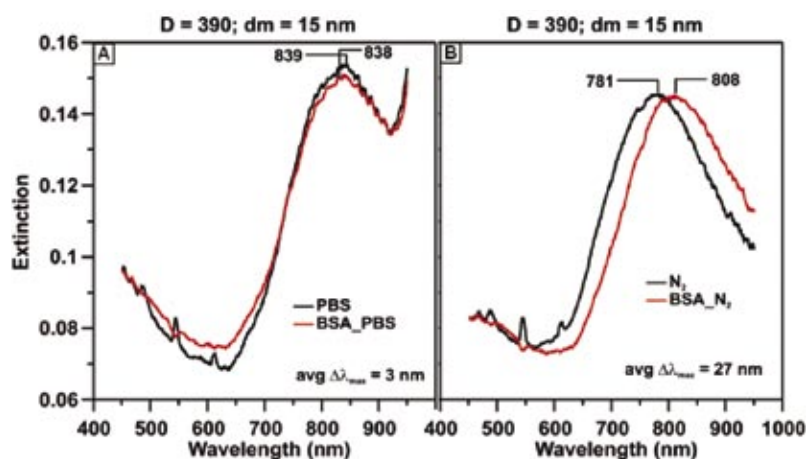


**Figure 11:** Nonspecific binding study on DNBA-functionalized Ag nanosensor. (a) LSPR measurements taken in PBS before and after incubation in BSA. (b) LSPR measurements taken in dry N<sub>2</sub> before and after incubation in BSA.

## Detection of Biological Analytes at Physiological Conditions Using Localized Surface Plasmon Resonance Spectroscopy (continued)

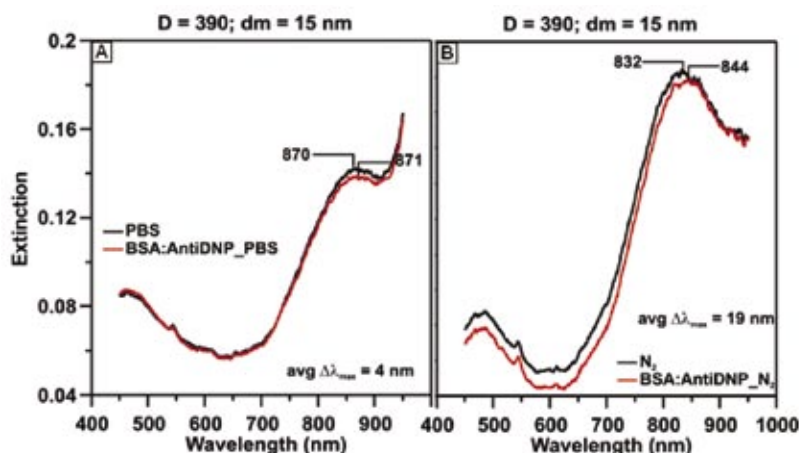


**Figure 12: Nonspecific binding study on DNBA-functionalized Ag nanosensor. (a) LSPR measurements taken in PBS before and after incubation in 1:1 BSA:antiDNP. (b) LSPR measurements taken in dry  $N_2$  before and after incubation in 1:1 BSA:antiDNP.**

antiDNP (Figure 7). The LSPR response was measured after the DNBA/antiDNP binding event took place: 719 nm in PBS and 713 nm in  $N_2$ . Thus, the shifts due to binding were about 15 nm in PBS (Figure 7A) and 20 nm in  $N_2$  (Figure 7B).

Figure 8 shows the LSPR response of the 50 nm height Ag nanoparticles. The  $\lambda_{\text{max}}$  measured in PBS was 671 nm before and 673 nm after exposure to  $4.912 \times 10^{-6}$  M antiDNP, a shift of 2 nm (Figure 8A). The  $\lambda_{\text{max}}$  measured in  $N_2$  was 631 nm before and 659 nm after incubation in antiDNP, resulting in a shift of 28 nm (Figure 8B).

The 15 nm sample experienced some experimental problems. Removal of the nanospheres without ripping off the Ag nanoparticles proved to be a challenge. Additionally, the concentration of antiDNP used for the 15 nm height samples was more than a degree

of magnitude smaller than that used in the 25 and 50 nm height samples. Regardless, the 25 and 50 nm height samples worked as expected. The antiDNP/DNBA binding event caused notable shifts in both the PBS and  $N_2$  spectra. Furthermore, the increased sensitivity in shorter nanoparticle heights is evident in the comparison of the 25 and 50 nm height samples.

The functionalizing of the 15 nm Ag particle surface with the SAM was confirmed by height changes in AFM measurements (Figure 9). The average height of the functionalized particles was 22 nm, corresponding to a 7 nm thick SAM.

### *Nonspecific Binding Study: Ag Nanoparticle Selectivity*

The LSPR response observed when antiDNP binds to the DNBA functionalized surface was verified by the following cases of a nonspecific binding study:

(1) *AntiDNP Activity with the Self-Assembled Monolayer (SAM) Only: No Functionalized-DNBA Surface.* The Ag nanosensors functionalized with SAMs only exhibited an LSPR  $\lambda_{\text{max}}$  of 842 nm in PBS and 799 nm in  $N_2$ . Incubation in  $1.05 \times 10^{-7}$  M antiDNP resulted in an LSPR  $\lambda_{\text{max}}$  of 839 nm in PBS and 802 nm in  $N_2$ . Thus, the LSPR response to antiDNP exposure was 3 nm in both PBS (Figure 10A) and in  $N_2$  (Figure 10B). Although there should be no  $\lambda_{\text{max}}$  shift, 3 nm falls within the error range.

(2) *BSA Interaction with the DNBA-Functionalized Sensor.* The DNBA-functionalized nanoparticle array experienced  $\lambda_{\text{max}}$  values of 839 nm in PBS and 781 nm in  $N_2$ . Exposing the nanosensor to BSA resulted in  $\lambda_{\text{max}}$  measurements of 839 nm in PBS and 808 nm in  $N_2$ . The LSPR response to the BSA solution was <1 nm in PBS (Figure 11A) and 27 nm in  $N_2$  (Figure 11B). The notable shift in  $N_2$  was assumed to be caused by insufficient rinsing of the sample. The remaining PBS particles would cause significant red-shifting in the  $N_2$  measurement.

(3) *Specific Sensing in the Presence of an Interfering Molecule.* The LSPR measurement of the DNBA-functionalized nanoparticles was 870 nm in PBS and 832 in  $N_2$ . When the sample was incubated in a 1:1 solution of BSA: $1.05 \times 10^{-7}$  M antiDNP, the LSPR  $\lambda_{\text{max}}$  was 871 nm in PBS and 844 in  $N_2$ . Therefore, the shift was only 1 nm in PBS (Figure 12a) and 12 nm in  $N_2$  (Figure 12b). We speculate that minimal shift occurred because the antiDNP concentration was too low.

## Conclusions

In this paper we have demonstrated that the NSL-fabricated Ag nanosensors are capable of detecting the binding event of antiDNP to a DNBA functionalized surface in buffer solution. The LSPR shift due to the binding event in the 25 nm height samples was approximately 10 nm in PBS. The 50 nm height samples experienced shifts of about 4 nm. This increased sensitivity in shorter nanoparticles is confirmed by the solvent study in which solvents of various refractive indices were exposed to the nanoparticle arrays. Additionally, the nonspecific binding study verified that the response seen when antiDNP binds the DNBA functionalized surface was due primarily to specific interactions. BSA did not bind the DNBA functionalized surface, and antiDNP did not bind the surface functionalized with the SAM only.

Future work will involve the multiplexing of LSPR nanosensors to examine the binding of several different molecules simultaneously on a single substrate. The schematic involves the selective functionalizing of the nanoparticle array through microfluidic channeling.

## References

- (1) Haes, A. J.; Van Duyne, R. P. *Expert Rev. Mol. Diagn.* **2004**, *4*, 527.
- (2) Haes, A. J.; Zou, S.; Schatz, G. C.; Van Duyne, R. P. *J. Phys. Chem. B* **2004**, *108*, 109.
- (3) Haes, A. J.; Zou, S.; Schatz, G. C.; Van Duyne, R. P. *J. Phys. Chem. B* **2004**, *108*, 6961.
- (4) Yonzon, C. R.; Jeoung, E.; Zou, S.; Schatz, G. C.; Mrksich, M.; Van Duyne, R. P. *J. Amer. Chem. Soc.* **2004**, *126*, 12669.
- (5) Sonnichsen, C.; Ludwig-Maximilians-University, Munich, 2001. Dissertation, submitted 20 June 2001.
- (6) Haynes, C. L.; Van Duyne, R. P. *J. Phys. Chem. B* **2001**, *105*, 5599.
- (7) Hutter, E.; Fendler, J. *Adv. Mater.* **2004**, *16*, 1685.
- (8) Stuart, D. A.; Haes, A. J.; Yonzon, C. R.; Hicks, E. M.; Van Duyne, R. P. *IEE Proc- Nanobiotechnol.* **2005**, *152*, 13.
- (9) Van Duyne, R. P. *Science* **2004**, *306*, 985.
- (10) Yonzon, C. R.; Zhang, X.; Van Duyne, R. P. *Proc. of SPIE* **2003**, *5224*, 78.
- (11) Jensen, T. R.; Duval, M. L.; Kelly, L.; Lazarides, A.; Schatz, G. C.; Van Duyne, R. P. *J. Phys. Chem. B* **1999**, *103*, 9846.
- (12) Malinsky, M. D.; Kelly, K. L.; Schatz, G. C.; Van Duyne, R. P. *J. Amer. Chem. Soc.* **2001**, *123*, 1471.
- (13) Malinsky, M. D.; Kelly, K. L.; Schatz, G. C.; Van Duyne, R. P. *J. Phys. Chem. B* **2001**, *105*, 2343.
- (14) Hulteen, J. C.; Van Duyne, R. P., J. *Vac. Sci. Technol. A* **1995**, *13*, 1553.
- (15) Mrksich, M.; Grunwell, J. R.; Whitesides, G. M. *J. Amer. Chem. Soc.* **1995**, *117*, 12009.
- (16) Murray, W. A.; Astilean, S.; Barnes, W. L. *Phys. Rev. B* **2004**, *69*, 165407.
- (17) Haes, A. J. C., L.; Klein, W. L.; Van Duyne, R. P. *J. Amer. Chem. Soc.* **2005**, *127*, 2264.